

Dynamics of basaltic glass dissolution – Capturing microscopic effects in continuum scale models

E.S.P. Aradóttir^{a,b,*}, B. Sigfússon^b, E.L. Sonnenthal^c, G. Björnsson^d, H. Jónsson^a

^a Science Institute, University of Iceland, Dunhaga 3, 107 Reykjavík, Iceland

^b Reykjavik Energy, Bæjarhálsi 1, 110 Reykjavík, Iceland

^c Lawrence Berkeley National Laboratory, 1 Cyclotron Rd, Berkeley, CA 94720, USA

^d Reykjavik Geothermal, Sudurlandsbraut 18, 108 Reykjavík, Iceland

Received 9 September 2011; accepted in revised form 16 April 2013; available online 15 July 2013

Abstract

The method of ‘multiple interacting continua’ (MINC) was applied to include microscopic rate-limiting processes in continuum scale reactive transport models of basaltic glass dissolution. The MINC method involves dividing the system up to ambient fluid and grains, using a specific surface area to describe the interface between the two. The various grains and regions within grains can then be described by dividing them into continua separated by dividing surfaces. Millions of grains can thus be considered within the method without the need to explicitly discretizing them. Four continua were used for describing a dissolving basaltic glass grain; the first one describes the ambient fluid around the grain, while the second, third and fourth continuum refer to a diffusive leached layer, the dissolving part of the grain and the inert part of the grain, respectively.

The model was validated using the TOUGHREACT simulator and data from column flow through experiments of basaltic glass dissolution at low, neutral and high pH values. Successful reactive transport simulations of the experiments and overall adequate agreement between measured and simulated values provides validation that the MINC approach can be applied for incorporating microscopic effects in continuum scale basaltic glass dissolution models. Equivalent models can be used when simulating dissolution and alteration of other minerals.

The study provides an example of how numerical modeling and experimental work can be combined to enhance understanding of mechanisms associated with basaltic glass dissolution. Column outlet concentrations indicated basaltic glass to dissolve stoichiometrically at pH 3. Predictive simulations with the developed MINC model indicated significant precipitation of secondary minerals within the column at neutral and high pH, explaining observed non-stoichiometric outlet concentrations at these pH levels. Clay, zeolite and hydroxide precipitation was predicted to be most abundant within the column.

© 2013 Elsevier Ltd. All rights reserved.

1. INTRODUCTION

Significant effort has been put into understanding the dissolution rates and alteration mechanisms of basaltic glass due to its widespread occurrence, e.g. on the ocean floor, in volcanic terrains and its emission during explosive

volcanic eruptions (e.g. Guy and Schott, 1989; Berger et al., 1994; Daux et al., 1997; Oelkers and Gíslason, 2001; Gíslason and Oelkers, 2003). Its role as a natural analog for various radioactive waste storage media is also relevant in this context (e.g. Daux et al., 1997; Techer et al., 2001, and references therein).

Generally, dissolution of natural basaltic glasses is believed to involve diffusion of metals through an alkali-depleted leached layer, which forms on particle surfaces (e.g. Oelkers and Gíslason, 2001; Gíslason and Oelkers, 2003;

* Corresponding author at: Reykjavik Energy, Bæjarhálsi 1, 110 Reykjavík, Iceland. Tel.: +354 516 6992; fax: +354 516 6709.

E-mail address: edda.sif.aradottir@or.is (E.S.P. Aradóttir).

Wolff-Boenisch et al., 2004). The fact that basaltic glass dissolution mechanisms are controlled by such microscopic processes complicates the application of continuum scale models for simulating its dissolution.

Reactive transport models provide versatile numerical laboratories for simulating coupled hydrological–geochemical evolution over a wide range of geological, industrial and experimental systems. Modern reactive transport models are based on mathematical formulation within the continuum (macroscopic) scale (e.g. Lichtner, 1996). Commonly used single porosity reactive transport models are, therefore, not designed to capture microscopic effects.

In this study, we attempt to bridge the gap between microscopic pore scale models and continuum scale reactive transport models by applying the method of ‘multiple interacting continua’ (Pruess and Narasimhan, 1985). The method is generally used to describe transport within fractures and matrix but the concept has been transferred to describing dissolution of individual basaltic glass particles. The method involves dividing the system up to ambient fluid and grains, using a specific surface area to describe the interface between the two. The various grains and regions within grains can be described by dividing them into continua separated by dividing surfaces. Millions of grains can thus be considered within the method without the need to discretize them explicitly.

In this study, a MINC-based basaltic glass dissolution model, which includes dissolution kinetics, leached layer formation and diffusion of ions through the leached layer, was constructed using the TOUGHREACT simulator (Xu et al., 2006, 2011). Transport and reaction mechanisms are defined separately in TOUGHREACT, which makes it possible to use different surface areas to describe internal diffusion and chemical reactivity of dissolving basaltic glass grains. The developed MINC model is capable of simulating reactive transport through a macroscopic, porous medium while still considering microscopic properties and gradients within individual basaltic grains.

A critical benchmark for any field of numerical modeling is its ability to accurately simulate well-constrained physical experiments, providing a necessary point of departure for predictive investigations (Johnson et al., 1998). The proposed MINC model was therefore validated using data from Sigfússon (2009), who carried out column flow through experiments of basaltic glass dissolution at low, neutral and high pH values.

2. THEORETICAL BACKGROUND

The dissolution of basaltic glass is considered to include two basic steps: (1) a first, provisional step of non-stoichiometric dissolution, due to the formation of a leached layer, followed by (2) a second step of steady-state, stoichiometric dissolution (Oelkers and Gíslason, 2001; Marini, 2007). In the first step, alkali and alkaline-earth metals are preferentially removed, leaving behind a leached layer enriched in Si and Al. Aluminum releasing exchange reactions between three aqueous H^+ and Al in the basaltic glass structure then partially remove Al from the remaining glass framework, followed by the relatively slow detachment of partially

liberated silica. Batch reactor experiments have shown that the time it takes to attain stoichiometric dissolution is short, or on the order of hours or days (e.g. Guy and Schott, 1989; Gíslason and Oelkers, 2003).

2.1. Dissolution mechanism

Gíslason and Oelkers (2003) measured the steady-state, far-from-equilibrium dissolution rate of basaltic glass in open system mixed flow reactors as a function of pH from 2 to 11 at temperatures from 6 to 50 °C, and at near neutral conditions from 6 to 150 °C. Measured dissolution rates displayed a common pH variation; decreasing dramatically with increasing pH under acid conditions, minimizing at near neutral pH, and increasing more slowly with increasing pH under alkaline conditions. In addition, the pH at which basaltic glass dissolution rate minimized decreased with increasing temperature.

By interpreting measured dissolution rates within the multioxide dissolution model, described, e.g. by Oelkers and Gíslason (2001), and applying regression, Gíslason and Oelkers concluded that dissolution of basaltic glass may be described within experimental uncertainty using:

$$r = A_A \exp \left[\frac{-E_A}{RT} \right] \left(\frac{a_{H^+}^3}{a_{Al^{3+}}} \right)^{1/3} \quad (1)$$

where r signifies the steady-state basaltic glass dissolution rate at far-from-equilibrium conditions, A_A refers to a constant equal to $10^{-5.6}$ (mol of Si)/cm²/s, E_A designates a pH independent activation energy equal to 25.5 kJ/mol, R is the universal gas constant, T is temperature in K and a_i represents the activity of the subscripted aqueous species, i .

Fig. 1 illustrates computed values of basaltic glass dissolution rates as a function of pH at temperatures from 0 to

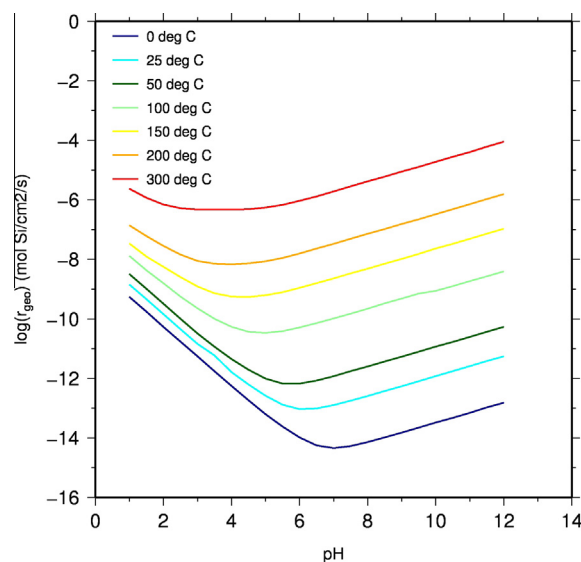
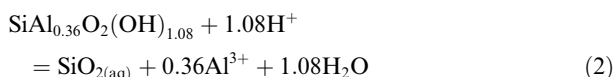


Fig. 1. Geometric dissolution rates of basaltic glass at temperatures from 0 to 300 °C, as predicted by the rate law of Gíslason and Oelkers (2003) shown in Eq. (1). Rates correspond to solutions having an ionic strength of 0.1 mol/kg, a total aqueous aluminum concentration of 10^{-6} mol/kg, and free of aluminum complexing aqueous species other than OH^- .

300 °C, as predicted by Eq. (1). Rates correspond to solutions having an ionic strength of 0.1 mol/kg, a total aqueous aluminum concentration of 10^{-6} mol/kg, and free of aluminum complexing aqueous species other than OH^- .

Gíslason and Oelkers (2003) used a basaltic glass deriving from volcanic ash from Stapafell, SW-Iceland, in their studies. The glass has the chemical formula normalized to one Si atom of $\text{SiTi}_{0.02}\text{Al}_{0.36}\text{Fe(III)}_{0.02}\text{Fe(II)}_{0.17}\text{Mg}_{0.28}\text{Ca}_{0.26}\text{Na}_{0.08}\text{O}_{3.38}$ (Oelkers and Gíslason, 2001). They assumed the following hydrolysis reaction for the hydrated leached layer:



2.2. Mathematical dissolution formulation in TOUGHREACT

The kinetic rate law used to describe mineral precipitation and dissolution in TOUGHREACT calculates kinetic rates as a product of the rate constant and reactive surface area, according to the following, which is based on transition state theory (Lasaga et al., 1994; Steefel and Lasaga, 1994):

$$r = kA \left[1 - \left(\frac{Q}{K} \right)^\theta \right]^\eta \quad (3)$$

where r is rate of dissolution or precipitation, k is the temperature dependent rate constant, A is the specific reactive surface area, K is the equilibrium constant for the dissolution/precipitation reaction taking place and Q is the reaction quotient. θ and η must be determined by experiment but are often set to unity (Xu et al., 2005b). Temperature dependence of the rate constant is given by an Arrhenius equation.

Combining Eqs. (1) and (3) and assuming θ and η are equal to unity yields the following equation that was used for simulating basaltic glass dissolution in the current study:

$$r = 10^{-5.6} A \exp \left[\frac{-E_A}{RT} \right] \left(\frac{a_{\text{H}^+}^3}{a_{\text{Al}^{3+}}} \right)^{1/3} \left(1 - \frac{Q}{K} \right) \quad (4)$$

2.3. Previous modeling approaches

Formation of a leached layer during dissolution of basaltic glass poses problems to geochemical model builders, as only Al and Si are released to the aqueous solution through the rate limiting dissolution of the hydrated leached layer (Eq. (2)). Preferentially removed alkali and alkaline earth metals are therefore neither accounted for chemically nor thermodynamically.

A common way to solve this problem is to use a so called ‘special reactant’ to take into account the fate of these metals (e.g. Marini, 2007). This second reactant would have the composition of $\text{Ti}_{0.02}\text{Fe(III)}_{0.02}\text{Fe(II)}_{0.17}\text{Mg}_{0.28}\text{Ca}_{0.26}\text{Na}_{0.08}\text{O}_{0.82}$, since it is the Si- and Al-free portion of the whole basaltic glass, and dissolves proportionally and

at the same rate as the hydrated basaltic glass. However, by using this approach, the problem is only partially solved, since the thermodynamic effects of the metals constituting the ‘special reactant’ are still not taken into account. The ‘special reactant’ method therefore might be too excessive a simplification.

Accornero and Marini (2008) studied the limitations of the method and found that the thermodynamic influences of the ‘special reactant’ become progressively higher as it comprises a larger proportion of the dissolving mineral or glass. The authors concluded that a special reactant should not include oxide components with molar fraction higher than 0.003, meaning that the method is not applicable to describing basaltic glass dissolution. The thermodynamic effects of the Si- and Al-free portion of the basaltic glass thus need to be taken into account when simulating basaltic glass dissolution.

2.4. Equilibrium constant for basaltic glass dissolution

Applying Eq. (4) for calculating basaltic glass dissolution rates requires defining equilibrium constants for the dissociation of the glass. Aradóttir et al. (2012a) estimated equilibrium constants for basaltic glass dissolution at temperatures ranging from 0 to 300 °C, applying a method based on a theoretical approach originally proposed by Paul (1977) that considers the glass to be an oxide mixture. Thus, the solubility of the material can be estimated from the ideal solid solution relation:

$$\log(K)_{\text{glass}} = \sum_i \log(K_i) + \sum_i x_i \log x_i \quad (5)$$

where x_i and K_i are the mole fractions and solubility products of the glass-constituting oxides.

This method of estimating solubility products of borosilicate and aluminosilicate glasses has already been successfully applied by, e.g. Bourcier et al. (1992), Advocat et al. (1998) and Leturcq et al. (1999). Techer et al. (2001) also obtained a good result using the same approach to model the dissolution of synthetic basaltic glass at 90 °C. Detailed description on the oxide dissolution reactions and $\log K_i$ values used for calculating equilibrium constants for the basaltic glass at different temperatures, along with justifications for methods used in the calculations can be found in Aradóttir et al. (2012a).

2.5. Mathematical description of transport processes

Transport is a fundamental part of the fluid–rock interaction processes described by reactive transport models for two reasons: (1) it provides the driving force for many of the reactions that take place by continuously introducing fluid out of equilibrium with respect to the reactive solid phase, and (2) it provides a characteristic time scale to be compared with the rates of reaction. Transport of mass and energy in TOUGHREACT is governed by advection and diffusion.

Advection involves the translation of fluid parcels over time. TOUGHREACT uses Darcy’s law to calculate fluid velocity in porous and fractured media:

$$\mathbf{F} = -k \frac{\rho}{\mu} (\nabla P - \rho \mathbf{g}) \quad (6)$$

where k is absolute permeability, ρ density, μ viscosity and $\mathbf{g} = (0,0,g)$ is the vector of gravitational acceleration. Dividing the mass flux by the fluid density gives the volumetric flux, \mathbf{u} , (i.e. the amount of fluid volume crossing a unit cross sectional area per unit of time). The volumetric flux is sometimes referred to as the Darcy velocity, but it is not the velocity with which the fluid parcels are actually flowing. The latter quantity is known as the pore velocity, denoted by \mathbf{v} :

$$\mathbf{u} = \phi \mathbf{v} \quad (7)$$

where ϕ is the porosity.

Diffusive mass flux in phase β is given by Fick's law, which assuming single-phase conditions reads:

$$\mathbf{F}_j = -D_j \nabla C_j \quad (8)$$

Here, ∇C_j is the concentration gradient of chemical component j , while D_j is the component's diffusion coefficient. Combining Eqs. (6) and (8) gives the full advection–diffusion equation used in TOUGHREACT:

$$\mathbf{F}_j = \mathbf{u} C_j - (\tau \phi S D_j) \nabla C_j \quad (9)$$

where τ is the tortuosity that represents the reduction in diffusion due to tortuous paths and S is the saturation index.

Eqs. (6)–(9) are used for describing transport of fluid and aqueous species within the MINC pore volume continuum in the current study. Transport of fluid and aqueous species within the leached layer and dissolving continuum does, however, only occur via diffusion.

3. MULTIPLE INTERACTING CONTINUA (MINC)

The method of ‘multiple interacting continua’ (MINC) is generally used to resolve transport of non-reactive chemicals in the fractured rock and its interaction with local exchange between fractures and matrix rock. This method was developed by Pruess and Narasimhan (1985) for fluid and heat flow in fractured porous media. Extension of the method to reactive geochemical transport is described in Xu and Pruess (2001). The MINC concept is based on the notion that changes in fluid pressure and chemical concentrations propagate rapidly through the fracture system, while invading the less permeable matrix blocks only slowly (Xu et al., 2001). Therefore, changes in matrix conditions will be locally controlled by the distance from the fractures and can then be modeled by means of one-dimensional nested grid blocks.

Although the MINC description above applies to the macroscopic interaction of matrix and fractures, the concept can be used for describing the microscopic behavior of individual particle parts during dissolution. A dissolving grain of basaltic glass can, e.g. be divided into three parts (assuming that it does not dissolve fully):

1. An outermost thin layer that is in full contact with ambient fluids and represents the leached layer, which ions diffuse through.

2. Within the diffusion layer lies the dissolving part of the grain. The dissolving part of the grain is to some extent exposed to ambient fluids via migration through irregularities/porosity in the outer layer, which studies show to be far from smooth (see Section 4).
3. The innermost part of the basaltic grain is inert and is not exposed to ambient fluids.

If the same dissolving basaltic glass grain is to be described by the MINC method, four continua are thus needed, as shown in Fig. 2; the first one describes the ambient fluid surrounding the grain, while the second, third and fourth continuum refer to the diffusive leached layer, the dissolving part of the grain and the inert part of the grain, respectively. If the basaltic glass grain were to dissolve fully, the inert part of the grain would be skipped and only three continua would be used for describing its dissolution.

By applying the MINC interpretation to model the dissolution of basaltic glass rather than a simple single or dual continuum setup, one can describe reactive flow through a porous medium while also taking into account gradients within individual dissolving particles as well as different rate limiting steps in dissolution mechanics. The MINC approach furthermore allows for describing millions of individual grains without explicitly discretizing them because of its ability to handle complex interfacial areas separating different domains within the grains. In the case of a 1D flow of water through a plug filled with basaltic glass grains, a conventional single continuum modeling approach would, e.g. only allow for describing water–basalt interaction through a reactive surface area that is solely used for calculating dissolution rates through Eq. (4). Upon dissolution, aqueous species are instantaneously released into the

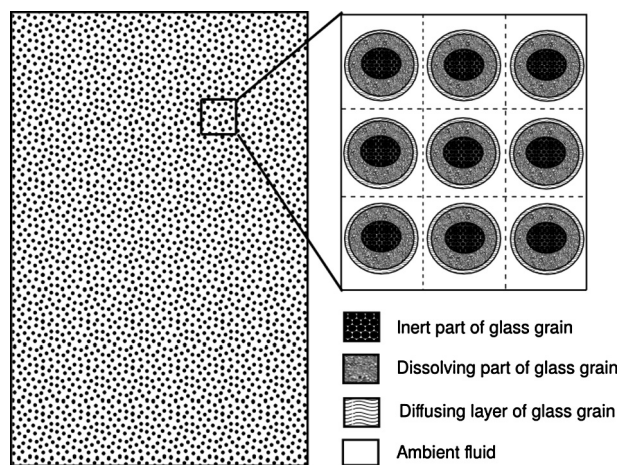


Fig. 2. The four-dimensional MINC interpretation of basaltic glass dissolution in the context of the column flow through experiments (see Section 4). The left figure shows a zoom-in of real grains in the plug, which is packed with basaltic glass grains of size 125–250 μm , yielding porosity of 0.45. The right top figure shows a blow up of several grain clusters within the plug and their interpretation as four interacting continua within the MINC approach. Each grain cluster consists of approximately 25,000 individual grains (1/80th of the total number of grains in the column).

surrounding fluid, not taking into account rate limiting steps such as diffusion through a leached layer and/or retention of specific metals. Diffusion would thus only be taken into account as a transport mechanism between different elements in the plug (interface area defined as cylindrical) but not as a transport property within individual basaltic grains (interface area defined as spherical geometric surface area). As a result, reaction rates tend to be significantly overestimated in numerical models when applying a single continuum approach for describing water–rock interactions in reactive transport models. Geochemical model builders often correct for such overestimates by reducing reported primary mineral rate constant values by several orders of magnitude when developing macroscopic models (see e.g. discussion in Aradóttir et al., 2012b). Such numerical “tricks” do, however, not tackle the underlying issue, i.e. that the dissolution rate is overestimated as a result of too a simple description of ongoing water–rock interactions. The MINC approach allows for including microscopic rate-limiting steps in such continuum scale macroscopic models.

4. EXPERIMENTAL DATA

Sigfússon (2009) carried out column flow through experiments on Stapafell glass at pH 3, 6.3, 8, 9 and 10. All experiments were carried out at 25 °C. Briefly, inlet solutions, stored in containers maintained under pressure with N₂ (Grade 5.0, BOC gases) were pumped to a vertical column and the outlet was then divided to a set of pH and Eh electrodes and a fraction collector for subsequent elemental analysis. Fig. 3 shows experimental setup in the column flow through experiments carried out by Sigfússon. Thin liquid flow lines represent PTFE tubing and thick liquid flow lines represent tubing for peristaltic pumps.

4.1. Column construction and tubing

The column was constructed from polytetrafluoroethylene (PTFE) with inner diameter of 1 cm, wall thickness of 1 cm and length of 16 cm. The column was closed in both ends with screw caps made from PTFE and a tight seal was provided by silicone o-rings. Nylon meshes were placed at each end the column to contain the basaltic glass. Tubing consisted of PTFE and valves were PTFE lined (Hamilton, Switzerland) except tubing compatible with the initial peristaltic pump head being Norprene (ColeParmer Masterflex) and Tygoon for the latter peristaltic pump head (Gilson). Additional outlets were placed into the experimental setup to vent any air from the flow line during initial stages of experiments. All column material and tubing was acid washed in 1 M HCl and rinsed with DI water prior to experiments.

4.2. Test solutions

Inlet column solutions were prepared from fresh 18.2 MΩ water and adjusted to pH values of 3, 6.3, 8, 9 and 10 and ionic strength of 10 mM by varying concentrations of HCl, NH₄Cl and NH₄OH according to Oelkers and

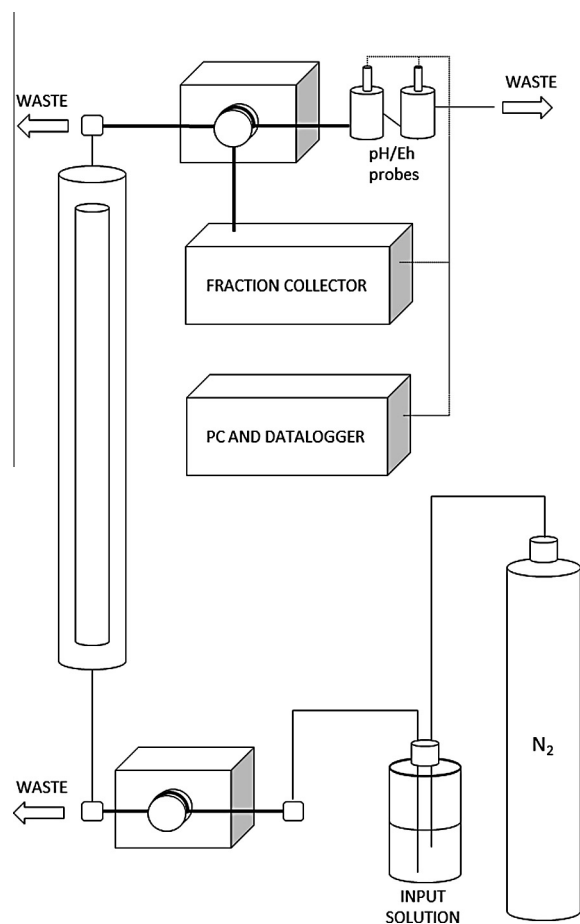


Fig. 3. Experimental setup in column flow through experiments carried out by Sigfússon (2009) on Stapafell basaltic glass at pH 3, 6.3, 8, 9 and 10. Thin liquid flow lines represent PTFE tubing and thick liquid flow lines represent tubing for peristaltic pumps.

Gíslason (2001). These solutions were purged for 2 h with grade 5.0 N₂ gas (BOC gases, Aberdeen) prior to startup of experiments and they were kept under N₂ pressure throughout the experimental duration preventing inflow of atmosphere to the experimental apparatus. Table 1 gives the compositions of solutions used in the column experiments.

4.3. Basaltic glass

Preparation of the glass was carried out according to Oelkers and Gíslason (2001). Grains of the 125–250 μm size

Table 1
Composition of solutions used in column flow through experiments (from Sigfússon (2009)). A small atmospheric contamination was allowed for in numerical simulations by assuming O₂ and CO₂ concentrations to be $2.0 \cdot 10^{-9}$ and $1.0 \cdot 10^{-6}$ mol/L, respectively.

pH (25 °C)	HCl (mol/L)	NH ₄ Cl (mol/L)	NH ₄ OH (mol/L)
3.00	0.00100	0.0090	
6.30	0.00010	0.0099	
8.02	0.00001	0.0095	0.0005
9.03		0.0065	0.0035
10.05		0.0015	0.0085

fraction were collected and an initial specific BET surface area measured to be $1.533 \pm 10\% \text{ m}^2/\text{g}$, which is 120 times larger than its estimated geometric surface area of $144 \text{ cm}^2/\text{g}$ (see below). 16 g of basaltic glass were packed into the column yielding a porosity of 45%.

SEM images of a glass grain before experiments are shown in Fig. 4. The figure shows that the initial basaltic glass grain is free of fine particles, and appears to be smooth on a micron scale. An enlargement of this image, shown in Fig. 4(b), reveals a large asperity on a 10–100 nm scale. This latter roughness may account, in part, for the large difference between the BET and geometric surface area of this glass powder. Other studies on Stapafell basaltic glass show similar difference between measured BET surface area and estimated geometric surface area (see, e.g. Oelkers and Gíslason, 2001; Gíslason and Oelkers, 2003).

4.4. Experimental procedure

A total of 1000 pore volumes were pumped at a rate of 1 ml/min through the column and then divided to pH and Eh sensors and a fraction collector, respectively. The fraction collector sampled outlet solutions at a rate of 0.5 ml/min in the following sampling sequence which was repeated throughout the experimental duration.

1. Solution was sampled for 10 min into a 6 ml high density polyethylene (HDPE) vial for the analysis of fluoride and sulfate by Dionex ICS-2000 ion chromatograph (separation on a Ionpac AS-11 column and 23 mM KOH eluent).
2. Solution was sampled for 10 min into a 15 ml HDPE vial for analysis of Si, Na, K, Ca, Mg, Fe, Al, Sr, Mn, Ti, S, P, Li, Mo, Cl, Br and B by a Spectro Ciros Vision ICP-AES. The solution was filtered through $0.2 \mu\text{m}$ cellulose acetate (CA) membrane (Advantec) and acidified to $\text{pH} < 1$ with concentrated HNO_3 (Merck, suprapure) prior to analysis.
3. Solution was sampled for 5 min into a 15 ml HDPE autosampler vial containing 0.25 ml of 5 M HCl for the analysis of ferrous (Fe(II)) and ferric (Fe(III)) iron by Dionex ICS-3000 ion chromatograph (separation on a Ionpac CS5A column with Metpac PDCA eluent and Metpac postcolumn reagent).

Three consecutive sampling cycles were carried out initially but thereafter a delay up to 8 h towards the end of the experiment was placed between sampling cycles. After each experiment, the material from the column was dried in N_2 gas flow for 24 h at ambient temperature prior to storage in an air-tight container. The surface of the basaltic glass was then coated with gold and analyzed (see Sigfússon et al., 2008, for figures and results).

5. MODEL SETUP

The results of Sigfússon (2009) provide a basis for testing the basaltic glass MINC model presented in Section 3. Hypothetically, each grain of basaltic glass used in the experiment could be described by the four continua described in Section 3. This would, however, have large computational requirements, as roughly 2 million particles of 125–250 μm size are needed to fill the column, after taking its 0.45 porosity into account. The corresponding MINC model would therefore require about 8 million elements, resulting in extremely long simulation times. In view of this, it was decided that rather than representing a single basaltic grain, each continua would represent a cluster containing ca. 25,000 individual grains (see below). Fig. 2 explains the four-dimensional MINC interpretation of basaltic glass dissolution in the context of the column flow through experiments carried out by Sigfússon (2009).

5.1. Model mesh and flow conditions

5.1.1. Elements and connections

Fig. 5 shows how elements and connections are set up within the MINC model of the column flow through experiment. The 16 cm column was divided into pore volume (45%, measured porosity) and glass volume (55%). The pore volume was further divided into 80 elements, each consisting of a 2 mm high cylinder. These cylinders serve as a flow channel for the solutions that are pumped through the column.

The glass volume was divided into three continua, each of which was further divided into 80 elements. The continua represent the diffusion layer of basaltic glass clusters, the dissolving part of basaltic glass clusters, and the inert part of basaltic glass clusters. Volumes of elements within the

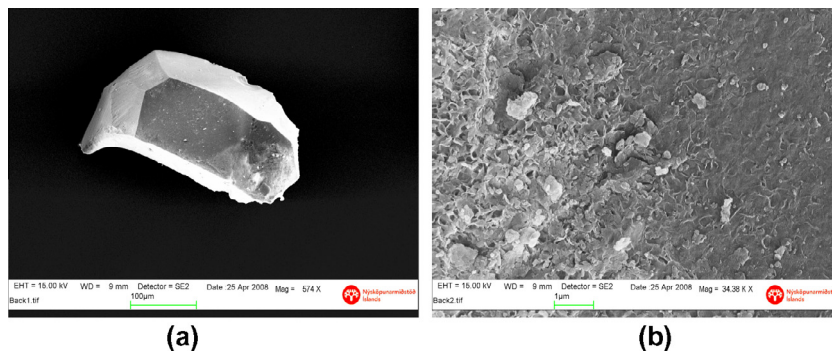


Fig. 4. Scanning electron micrographs of the basaltic glass used in the present study. Figure (b) is a magnified view of figure (a) revealing large asperity on the 10–100 nm scale.

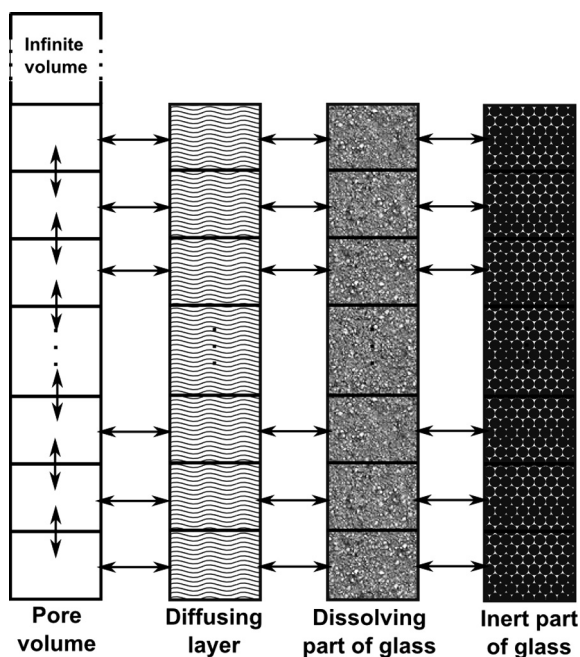


Fig. 5. Schematic illustration of elements and connections in the four-dimensional MINC setup. Columns represent different continua, each of which has 80 elements (represented by boxes). Arrows show connections between elements and continua. Interfacial areas for connections between continua are given in Table 2.

different continua were calculated using the average experimental grain size ($187.5\ \mu\text{m}$) and assuming a spherical grain shape. Areas connecting elements within different continua were calculated assuming spherical shapes as well (i.e. geometric surface areas). The porous leached layer and dissolving part of grains were presumed to be $100\ \text{nm}$ and $20\ \mu\text{m}$ thick, respectively. The leached layer thickness was based on values reported by Nesbitt and Skinner (2001), whereas the thickness of dissolving grain parts was roughly determined from the total amount of glass dissolved in column flow through experiments.

Each glass volume continuum interacts with its outer surroundings through its surface area which was calculated assuming spherical grain shape. Diffusion from the dissolving part of glass grains through the diffusion layer and out towards the flow channel is therefore calculated using geometric surface areas. The chemical reactivity of the dissolving part of glass grains was however described using the BET surface area measured by Sigfússon (2009). The reactive properties of the glass can be separated from its transport properties (i.e. its diffusivity) as these two mechanisms are described separately in the input to TOUGHREACT.

5.1.2. Flow conditions

As the pore volume cylinder serves as a flow channel for the solutions that flow through the column, elements within the pore volume are interconnected. Each element in the pore volume is also connected to an element from the diffusive leached layer continuum with an interface area corresponding to the surface area of grains within that single

element (1/80th of the total basaltic glass needed to fill the column). Each element within the diffusion continuum is also connected to an element from the dissolving continuum, which is in turn connected to an element from the inert glass continuum. Elements within the diffusive continuum are not interrelated, and hence, touching of grain clusters within the column is neglected.

A single inactive element of infinite volume was placed at the top of the pore volume continuum to prevent pressure from building up from within the column (see Fig. 5). This element does not contain any basaltic glass. The tortuosity of the second topmost pore volume element was also set to a low value, and the distance to its interface common with the infinite volume element increased. This was done in order to prevent numerical back diffusion from the inactive element into active elements below. To ensure that back diffusion would not affect simulated results, the model output that is compared with measured values was assumed to be at the third element from the top.

Table 2 summarizes the physical properties of elements and connections of the four continua used in the MINC model.

5.1.3. Averaging within the integral finite difference method

TOUGHREACT, like other members of the TOUGH family of codes, applies the integral finite difference method (Edwards, 1972; Narasimhan and Witherspoon, 1976), resulting in values being averaged between adjacent grid points. This means that strictly speaking three diffusion layers are needed for accurate diffusion to occur between the pore volume and the dissolving continuum because values are averaged between the continua. This, however, increases the number of elements in the model significantly, resulting in larger computational requirements. Using three layers can be avoided by fixing the diffusivity in the continua by changing their tortuosity so that the product of their porosity, tortuosity and diffusion coefficient remains constant. This numerical trick was applied in the current study to keep the number of elements at a minimum.

5.2. Geochemical system

5.2.1. Mineral selection and thermodynamic data

Aradóttir et al. (2012a) developed and evaluated a thermodynamic database describing mineral reactions of interest for basaltic alteration. Selection of primary and secondary minerals in the database was based on extensive review of natural analogs of water–basalt interaction. The thermodynamic database of Aradóttir et al. (2012a) was compiled and used in the simulations carried out in the current study. The EQ3/6 V7.2b database (Wolery, 1992) is the primary source for aqueous equilibrium constants in the database but reactions for four Al-hydroxy complexes were added. Methods used for compiling and validating the thermodynamic database are extensively discussed in Aradóttir et al. (2012a). All mineral dissolution/precipitation reactions were written in terms of the same basis species set as used by Aradóttir et al. (2012a).

Basaltic glass is the only primary mineral used in the MINC model developed here, filling the three continua

Table 2
Physical properties of elements and connections of the four continua used in the MINC dissolution model.

	↑ Connections within pore volume ↓	Pore volume	← Connections →	Diffusion layer ^a	← Connections →	Dissolving part ^b of grains	← Connections →	Inert part of grains
<i>Elements</i>								
Porosity (ϕ)		1.00		0.02		0.01		0.00
Permeability (k (mD))		600		600		600		600
Tortuosity (τ^c)		0.002		0.1		0.02		0.2
Diffusion coeff. (m ² /s)		$2.0 \cdot 10^{-9}$		$2.0 \cdot 10^{-9}$		$2.0 \cdot 10^{-9}$		$2.0 \cdot 10^{-9}$
$V_{\text{one element}}$ (m ³) ^d		$7.7 \cdot 10^{-8}$		$2.8 \cdot 10^{-10}$		$4.4 \cdot 10^{-8}$		$4.2 \cdot 10^{-8}$
<i>Connections</i>								
Interface area (m ²)	$3.5 \cdot 10^{-5e}$		$1.6 \cdot 10^{-3f}$		$1.6 \cdot 10^{-3f}$		$1.3 \cdot 10^{-3f}$	
Δx_1 (m) ^g	$1 \cdot 10^{-3}$		0 ^h		$5 \cdot 10^{-8}$		$1 \cdot 10^{-5}$	
Δx_2 (m) ^g	$1 \cdot 10^{-3}$		$8 \cdot 10^{-9i}$		$1 \cdot 10^{-5}$		$4 \cdot 10^{-5}$	

^a Assumed to be 100 nm thick. BET surface defines reactivity but geometric surface defines diffusion properties.

^b Assumed to be 20 μm thick.

^c Fix diffusivity between continua by keeping the product of porosity and tortuosity constant and thereby avoid parameter weighting between continua (see discussion in Section 5.1 for more detail).

^d Calculated using the average particle size from Sigfússon (2009) and assuming spherical shape of grains.

^e Area of circle corresponding to column cross-section.

^f Geometric surface area of grains within a single element calculated from average particle size (1/80th of the total basaltic glass needed to fill the column).

^g Distance between first and second element, respectively, to their common interface.

^h Pore volume treated as a fracture.

ⁱ 1/6th of correct value according to Zimmerman et al. (1992).

describing glass grains. Ferric iron (Fe_2O_3) was stoichiometrically replaced with ferrous iron (FeO) as using both oxidation states as primary species can cause problems in numerical simulations. Equilibrium and supply of $\text{O}_{2(aq)}$ governs oxidation of Fe(II) dissolved from primary minerals to Fe(III) in the simulations. Basaltic glass composition was taken from Oelkers and Gíslason (2001). TiO_2 and P_2O_5 , which make up 1.564 and 0.195 weight % of the total glass composition, respectively, were ignored. This was done because titanium and phosphorus are not included in the system being modeled in the current study.

All secondary minerals from the database of Aradóttir et al. (2012a) were compiled as potential secondary minerals, as shown in Table 3. Compositions of solutions used in simulations of the column flow through experiments were the same as given in Table 1. A small atmospheric contamination was however allowed for in the solutions, even though the experimental solutions were purged with N_2 , by assuming O_2 and CO_2 concentrations to be $2.0 \cdot 10^{-9}$ and $1.0 \cdot 10^{-6}$ mol/L, respectively. Precipitation was set up in such a way that it can only occur in the pore volume continuum while basaltic glass dissolution occurs in the dissolving continuum. No secondary minerals were present in the column when starting column flow through simulations.

5.2.2. Kinetics of mineral dissolution and precipitation

Precipitation and potential re-dissolution of all minerals except allophane, $\text{Al(OH)}_{3(am)}$, antigorite, calcite, Fe(II) and Fe(III) hydroxides, imogolite and kaolinite is kinetically controlled. Kinetic rates are a product of the rate constant and reactive surface area, according to rate expression (3), which is transition state theory based. As dissolution and precipitation of minerals are often catalyzed by H^+ (acid mechanism) or OH^- (base mechanism), the rate constant in Eq. (3) can be written as the sum of three mechanisms:

$$r = k_{25}^{\text{nu}} \exp \left[\frac{-E_A^{\text{nu}}}{R} \left(\frac{1}{T} - \frac{1}{298.15} \right) \right] + k_{25}^{\text{H}} \exp \left[\frac{-E_A^{\text{H}}}{R} \left(\frac{1}{T} - \frac{1}{298.15} \right) \right] a_{\text{H}}^{n_{\text{H}}} + k_{25}^{\text{OH}} \exp \left[\frac{-E_A^{\text{OH}}}{R} \left(\frac{1}{T} - \frac{1}{298.15} \right) \right] a_{\text{OH}}^{n_{\text{OH}}} \quad (10)$$

where nu, H and OH denote neutral, acid and base mechanisms, respectively. E_A is activation energy, k_{25} the rate constant at 25 °C, R is the gas constant, T absolute temperature and a activity of a species.

Table 3
Chemical composition of the minerals and aqueous species considered in this study.

Group	Mineral	Chemical composition	
Primary minerals	Basaltic glass	$\text{SiAl}_{0.36}\text{Fe(II)}_{0.19}\text{Mg}_{0.28}\text{Ca}_{0.26}\text{Na}_{0.08}\text{O}_{3.31}$	
Silicates	Allophane	$\text{Al}_2\text{O}_3(\text{SiO}_2)_{1.22}(\text{H}_2\text{O})_{2.5}$	
	Amorphous silica	SiO_2	
	Antigorite	$\text{Mg}_3\text{Si}_2\text{O}_5(\text{OH})_4$	
	Ca-Montmorillonite ^a	$\text{Ca}_{0.167}\text{Al}_{1.67}\text{Mg}_{0.33}\text{Si}_4\text{O}_{10}(\text{OH})_2$	
	Celadonite ^b	$\text{KMgAlSi}_4\text{O}_{10}(\text{OH})_2$	
	Fe-Celadonite ^b	$\text{KFeAlSi}_4\text{O}_{10}(\text{OH})_2$	
	Fe-Chlorite ^b	$\text{Fe}_5\text{Al}_2\text{Si}_3\text{O}_{10}(\text{OH})_8$	
	Imogolite	$\text{Al}_2\text{SiO}_3(\text{OH})_4$	
	Kaolinite	$\text{Al}_2\text{Si}_2\text{O}_5(\text{OH})_4$	
	K-Montmorillonite ^a	$\text{K}_{0.33}\text{Al}_{1.67}\text{Mg}_{0.33}\text{Si}_4\text{O}_{10}(\text{OH})_2$	
	Mg-Chlorite ^b	$\text{Mg}_5\text{Al}_2\text{Si}_3\text{O}_{10}(\text{OH})_8$	
	Mg-Montmorillonite ^a	$\text{Al}_{1.67}\text{Mg}_{0.5}\text{Si}_4\text{O}_{10}(\text{OH})_2$	
	Moganite	SiO_2	
	Na-Montmorillonite ^a	$\text{Na}_{0.33}\text{Al}_{1.67}\text{Mg}_{0.33}\text{Si}_4\text{O}_{10}(\text{OH})_2$	
	Quartz	SiO_2	
	Hydroxides	Amorphous Al hydroxide	$\text{Al}(\text{OH})_3$
		Fe(II) hydroxide	$\text{Fe}(\text{OH})_2$
		Fe(III) hydroxide	$\text{Fe}(\text{OH})_3$
	Carbonates	Calcite	CaCO_3
		Dolomite	$\text{CaMg}(\text{CO}_3)_2$
Magnesite ^b		MgCO_3	
Siderite ^b		FeCO_3	
Zeolites	Analcime	$\text{Na}_{0.96}\text{Al}_{0.96}\text{Si}_{2.04}\text{O}_6 \cdot \text{H}_2\text{O}$	
	Ca-Chabazite ^c	$\text{CaAl}_2\text{Si}_4\text{O}_{12} \cdot 6\text{H}_2\text{O}$	
	Ca-Heulandite ^c	$\text{CaAl}_2\text{Si}_7\text{O}_{18} \cdot 6\text{H}_2\text{O}$	
	Laumontite	$\text{CaAl}_2\text{Si}_4\text{O}_{12} \cdot 4.5\text{H}_2\text{O}$	
	Mesolite	$\text{Ca}_{0.666}\text{Na}_{0.666}\text{Al}_2\text{Si}_3\text{O}_{10} \cdot 2.667\text{H}_2\text{O}$	
	Na-Chabazite ^c	$\text{Na}_2\text{Al}_2\text{Si}_4\text{O}_{12} \cdot 6\text{H}_2\text{O}$	
	Na-Heulandite ^c	$\text{Na}_2\text{Al}_2\text{Si}_7\text{O}_{18} \cdot 5\text{H}_2\text{O}$	
	Natrolite	$\text{Na}_2\text{Al}_2\text{Si}_3\text{O}_{10} \cdot 2\text{H}_2\text{O}$	
	Stellerite ^d	$\text{Ca}_2\text{Al}_4\text{Si}_{14}\text{O}_{36} \cdot 14\text{H}_2\text{O}$	
	Stilbite ^d	$\text{Ca}_2\text{NaAl}_5\text{Si}_{13}\text{O}_{36} \cdot 16\text{H}_2\text{O}$	

^a Forms a solid solution between Ca, K, Mg and Na end-members.

^b Forms a solid solution between Mg and Fe end-members.

^c Forms a solid solution between Ca and Na end-members.

^d Stellerite and stilbite form a solid solution.

The rate law of Gíslason and Oelkers (2003), given by Eq. (1), was implemented in TOUGHREACT using a general form of a species dependent rate constant that is coded in TOUGHREACT:

$$r = k_{25}^{\text{su}} \exp \left[\frac{-E_a^i}{R} \left(\frac{1}{T} - \frac{1}{298.15} \right) \right] + \sum_i k_{25}^i \times \exp \left[\frac{-E_a^{\text{H}}}{R} \left(\frac{1}{T} - \frac{1}{298.15} \right) \right] a_{\text{H}}^{\text{H}} \prod_j a_j^{ij} \quad (11)$$

where i denotes the species dependent mechanism and j specific species to which the rate constant depends on.

Parameters used for the kinetic rate expression of different minerals are given in Table 4. Rate-law parameters for moganite and quartz were taken from Gíslason et al. (1997) and from Rimstidt and Barnes (1980) for $\text{SiO}_{2(\text{am})}$. Rate law parameters for other minerals are from Palandri and Kharaka (2004). All zeolites were assumed to have the same rate law as heulandite due to lack of data in the literature.

In the current study, the reactive surface area of the primary basaltic glass was that measured by Sigfússon (2009) in his column flow through experiments. Surface areas of precipitated minerals are, however, generally unknown and this causes problems for geochemical model builders. In the current study, surface areas of secondary clay minerals, zeolites and carbonates were assumed to be 10,000, 1000 and 500 cm^2/g , respectively. Secondary $\text{SiO}_{2(\text{s})}$ minerals were assumed to have a surface area of 1,000 cm^2/g .

When the aqueous phase supersaturates with respect to a certain secondary mineral, a small volume fraction of $1 \cdot 10^{-6}$ was used for calculating a seed surface area for the new phase to grow. This approach is commonly used in reactive transport simulations (see, e.g. Xu et al. (2010)). The precipitation of secondary minerals is represented using the same kinetic expression as that for dissolution, except for $\text{SiO}_{2(\text{am})}$ which precipitates under the free energy rate law of Carroll et al. (1998). As precipitation rate data for most minerals are unavailable, parameters for neutral pH dissolution rates were employed to describe precipitation. This is a critical but necessary assumption because of lack of data on precipitation kinetics.

6. SIMULATIONS

Reactive transport simulations of the column flow through experiments were carried out with the MINC model shown in Fig. 5 and TOUGHREACT at pH 3, 6.3, 8, 9 and 10, using the same flow rate as Sigfússon (1 ml/min). Mass transport and batch geochemical simulations of water–rock interaction were carried out before starting fully coupled reactive mass transport simulations in order to get steady-state fluid flow conditions and to equilibrate initial water with the basaltic glass. Boundary water compositions are given in Table 1.

7. RESULTS

Fig. 6 shows comparison of steady-state measured and simulated column output for pH and selected species. Agreement between measured and simulated Al concentrations is good at all pH levels. Measured and simulated outlet pH also exhibit a good match, except around neutral pH where the model predicts significantly higher values. Measured and simulated Mg and Fe concentrations are close to zero at all pH levels apart from pH 3, indicating these species to precipitate into secondary minerals. Simulated SiO_2 concentrations are somewhat higher than measured values at all pH levels apart from pH 10, and the same applies to simulated Ca concentrations at pH 6.3, 9 and 10.

Table 4

Initial rock mineral composition and potential alteration minerals along with parameters for calculating kinetic rates for mineral dissolution and precipitation.

Mineral ^a	Vol% of solid	<i>A</i> (cm ² /g)	Parameters for kinetic rate law							
			Neutral mechanism		Acid mechanism			Base mechanism		
			<i>k</i> ₂₅ (mol/m ² /s)	<i>E</i> _A (kJ/mol)	<i>k</i> ₂₅ (mol/m ² /s)	<i>E</i> _A (kJ/mol)	<i>n</i> (H ⁺)	<i>k</i> ₂₅ (mol/m ² /s)	<i>E</i> _A (kJ/mol)	<i>n</i> (H ⁺)
<i>Primary</i>										
Basaltic glass	100	15,330	<i>k</i> ₂₅ = 4.096 H 10 ⁻⁷ <i>E</i> _A = 25.5 <i>n</i> (H ⁺) = 1.00, <i>n</i> (Al ⁺³) = -0.33							
<i>Secondary</i>										
Celadonite ^b		10,000	1.660 · 10 ⁻¹³	35.0	1.047 · 10 ⁻¹¹	23.6	0.34	3.020 · 10 ⁻¹⁷	58.9	-0.40
Montmorillonite ^b		10,000	3.890 · 10 ⁻¹⁵	48.0	1.950 · 10 ⁻¹²	48.0	0.220	3.890 · 10 ⁻¹²	78.0	-0.130
Moganite ^c		1,000	1.653 · 10 ⁻¹³	70.5						
Quartz ^c		1,000	1.223 · 10 ⁻¹²	80.5						
SiO ₂ (<i>am</i>) ^d		1,000	7.32 · 10 ⁻¹³	60.9						
Dolomite ^b		500	2.951 · 10 ⁻⁸	52.2	6.457 · 10 ⁻⁴	14.4	1.0			
Magnesite ^b		500	4.571 · 10 ⁻¹⁰	23.5	4.169 · 10 ⁻¹⁰	14.4	1.0			
Siderite ^e		500	1.259 · 10 ⁻⁹	62.76	1.590 · 10 ⁻⁴	45.0	0.9	2.512 · 10 ⁻¹⁶	71.0	-0.572
Zeolites ^f		1,000	1.585 · 10 ⁻¹²	58.0	1.995 · 10 ⁻⁸	58.0	0.70	5.495 · 10 ⁻¹⁵	58.0	-0.30

^a Allophane, Al(OH)₃(*am*), antigorite, calcite, Fe(II) and Fe(III) hydroxides, imogolite and kaolinite precipitate under equilibrium.

^b From Palandri and Kharaka (2004).

^c From Gíslason et al. (1997).

^d From Rimstidt and Barnes (1980). Precipitation occurs under the free energy rate law of Carroll et al. (1998).

^e From Knauss et al. (2005).

^f All zeolites assumed to have the same rate law as heulandite from Palandri and Kharaka (2004).

The MINC model predicts precipitation of secondary minerals to be negligible in simulations at pH 3 but considerable at neutral and high pH. Chlorite, which is Mg-, Al- and Fe-rich, is the most common secondary mineral but stellerite–stilbite solid solution, Al-hydroxide, kaolinite, celadonite, heulandite and imogolite also form in smaller amounts. The model predicts precipitation to occur throughout the whole plug, but to be most abundant near the inlet, where dissolution is most extensive. Some minerals, such as stellerite–stilbite, precipitate primarily towards the outlet of the column. Fig. 7 shows modeled chlorite and stellerite–stilbite volume abundance throughout the plug at different pH levels. Chlorite abundance increases with higher pH, while stellerite–stilbite abundance increases from pH 3 to pH 6.3 but then decreases again at higher pH. At neutral pH, Mg and Fe content is similar in the precipitated chlorite, but Mg content increases at higher pH. The chemical composition of precipitated stellerite–stilbite is near the end-member stellerite.

Fig. 8 shows simulated pH as a function of column length at the end of the flow through experiments. pH rises gradually throughout the plug in experiments carried out at pH 3, while it rises quickly near the plug inlet in experiments carried out at pH 6.3 and pH 8. pH is fairly steady throughout the plug in experiments carried out at pH 9 and 10. Similar figures drawn earlier in the simulation of the plug flow experiments show very similar trends. Changes in pH along the column length do not follow the same trend as the buildup of secondary minerals shown in

Fig. 7, but rather follow the amount of basaltic glass dissolved at specific length intervals within the plug. Basaltic glass dissolution is simulated to be most extensive near the plug's front, gradually becoming smaller along the plug's length. It thus seems like pH in the column is governed by the amount of glass dissolved but not the amount of secondary minerals precipitated. Experimental setup only allowed for taking samples at the plug's outlet so it was not possible to compare the results shown in Fig. 8 to measurements.

Fig. 9 shows the steady state measured outlet Fe(III) concentration versus total Fe concentration in the column outlet as a function of inlet pH. Fe(III) accounts for about 10% of the total Fe in Stapafell basaltic glass (Oelkers and Gíslason, 2001). Fig. 9 exhibits similar ratio at pH 3, indicating Fe(II) and Fe(III) to be stoichiometrically released. At pH 6.3, 8 and 9, however, the median of Fe(III) vs. total Fe ratio is 100%, implying only Fe(III) to be released from the column at these pH levels. At pH 10, the median of Fe(III) vs. total Fe ratio is around 5%.

Fig. 10 shows the relative mobility of Al, Ca, Fe, K, Mg and Na with respect to Si in column outlet solutions. Contrary to the results of Oelkers and Gíslason (2001), column outlet concentrations are only close to being stoichiometric at pH 3. Na and Si are released stoichiometrically from the column at pH 3, while Na has significantly higher mobility at pH 6.3 and concentration below detection limit at higher pH. K is highly mobile in the beginning of all experiments and remains high at pH 10. The relative mobility of K

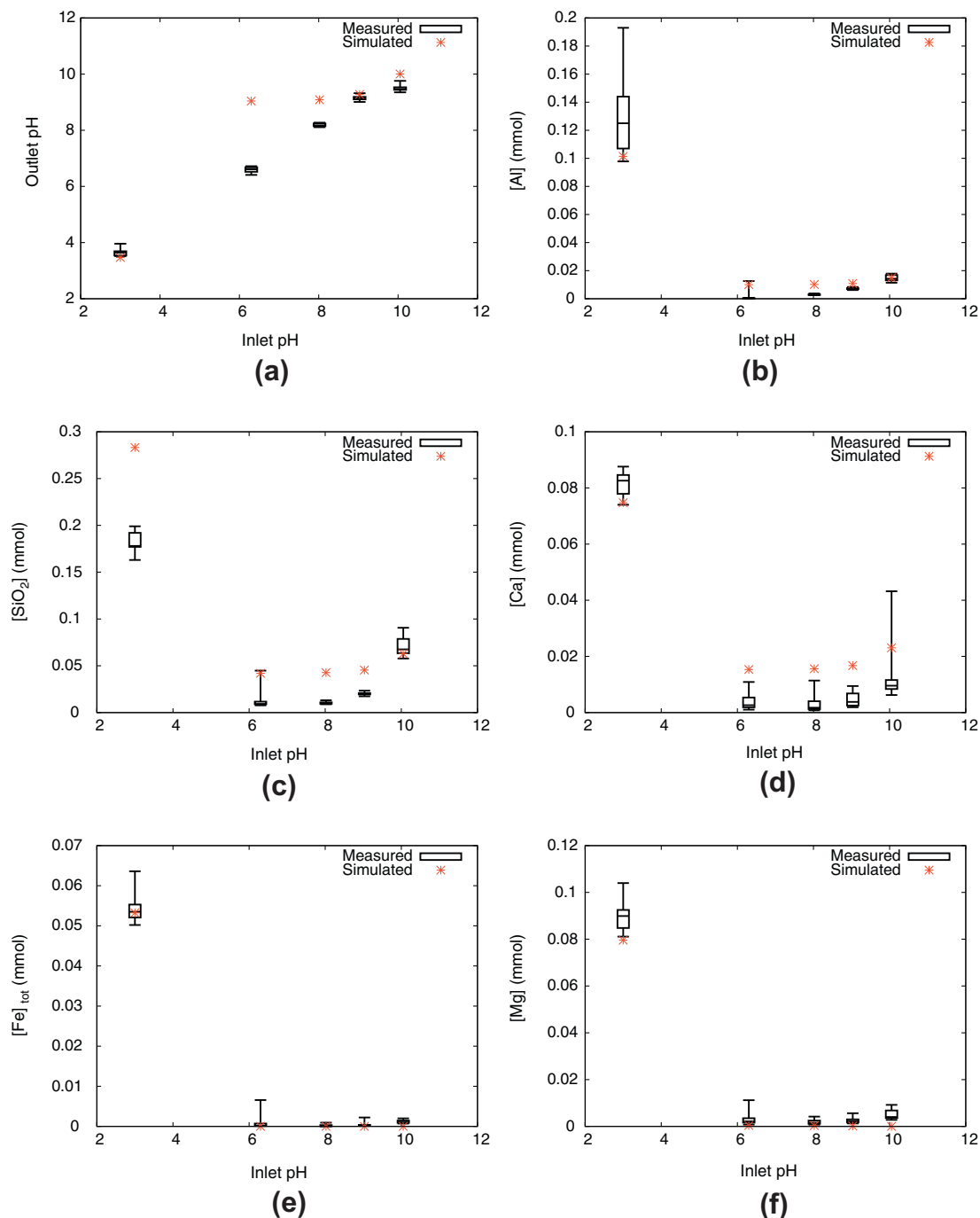


Fig. 6. Comparison of measured and simulated column output. Stars represent simulated values, whereas the box-and-whisker diagrams show the five-number summaries of steady-state measured values (sample minimum, lower quartile, median, upper quartile and sample maximum).

decreases with time at lower pH and outlet concentrations are generally below detection limits. Mg and Ca column outlet concentrations are stoichiometric compared to Si at pH 3 and same applies to Ca at pH 10. Steady state relative mobilities of Mg and Ca gradually decrease to values lower than unity at other pH levels. Al and Si are released stoichiometrically from the column at all pH except pH 6.3, where Al is substantially less mobile.

8. DISCUSSION

The MINC model predicts higher outlet pH values than measured around neutral inlet pH, as shown in Fig. 6. This suggests that the model either overestimates glass dissolution or underestimates precipitation of secondary minerals. The fact that simulated SiO₂ and Ca concentrations tend to be higher than measured values supports the theory that

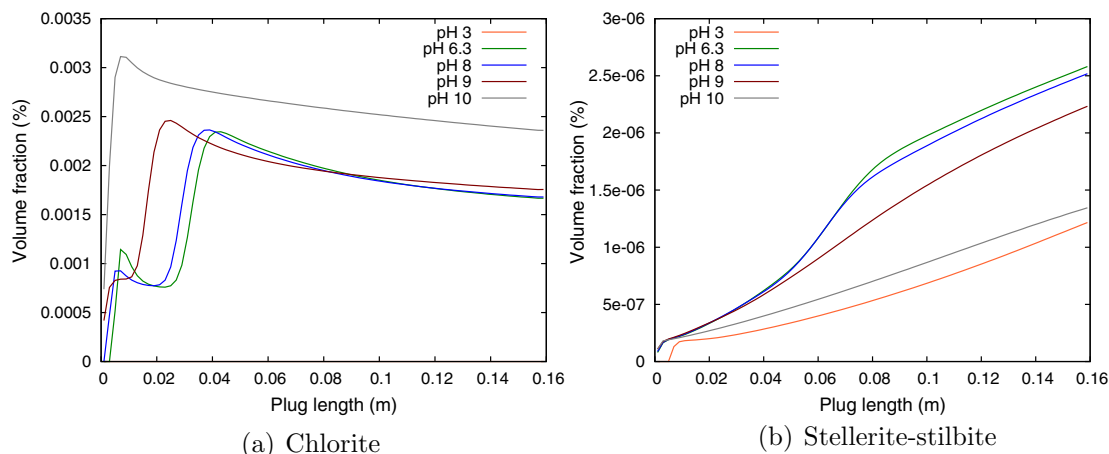


Fig. 7. Chlorite and stellerite–stilbite volume abundance throughout the plug as predicted by the MINC model. Chlorite precipitation is three orders of magnitude greater than of stellerite–stilbite.

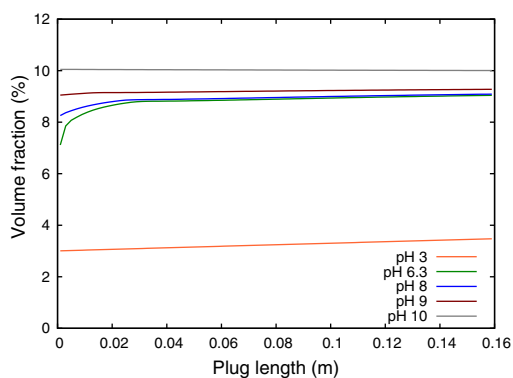


Fig. 8. Simulated pH as a function of column length at the end of plug flow through experiments. pH rises gradually throughout the plug in experiments carried out at pH 3, while it rises quickly near the plug inlet in experiments carried out at pH 6.3 and pH 8. pH is fairly steady throughout the plug in experiments carried out at pH 9 and 10.

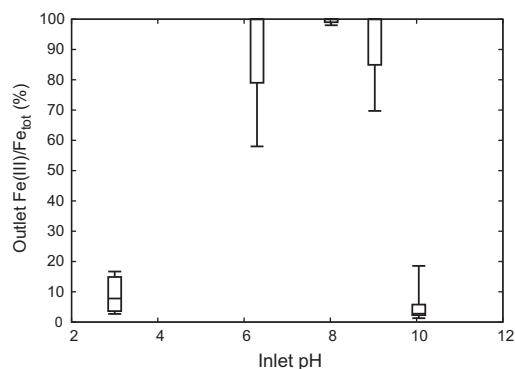


Fig. 9. Steady state measured outlet Fe(III) concentration versus total Fe concentration in column outlet as a function of inlet pH. Data is represented by box-and-whisker diagrams, which show the five-number summaries of measured values (sample minimum, lower quartile, median, upper quartile and sample maximum).

abundance of Si- and Ca-rich secondary minerals is underestimated by the model. As zeolites and calcite are the only Ca-rich weathering products commonly found in basaltic glass (Stefánsson and Gíslason, 2001), indications are that zeolite precipitation is underestimated in the numerical model. Zeolite rate-law parameters are scarcely found within the literature and this is why all zeolites in this study were assumed to have the same rate-law parameters as reported for heulandite. Improved knowledge on the kinetics rate-laws of different zeolites is likely to improve numerical models. Simulated Mg and Fe concentrations are both close to zero as shown in Fig. 6. Simulated concentrations are, however, generally one order of magnitude lower than the measured outlet concentrations. A possible explanation for that is that the secondary Mg and Fe phases were too stable relative to the actual minerals due to uncertainties in corresponding equilibrium constants, possibly due to nonideality in the actual precipitating solid solution clay minerals. At concentrations close to zero, such uncertainties can significantly affect simulated concentrations.

High relative mobility of Na to Si at pH 6.3 implies the precipitation of a Si-rich mineral, such as $\text{SiO}_{2(am)}$ or a Na-free zeolite. Stellerite is among Na-free zeolites and simulations predict stellerite precipitation to be at a maximum at pH 6.3 (see Fig. 7). The non-stoichiometric behavior of Al at pH 6.3 can furthermore be explained by precipitation of amorphous Al-hydroxide as the solubility of $\text{Al}(\text{OH})_{3(am)}$ is at a minimum at this particular pH level (Langmuir, 1997). The simulations carried out in this study support this hypothesis, as Al-hydroxide is predicted to be the third most abundant secondary mineral to form at pH 6.3 after chlorite and stellerite–stilbite.

This study shows that reactive transport modeling can give further insight into experiments performed in laboratories or in the field, especially when dealing with dynamic processes and systems. Simulations of the column flow through experiment carried out by Sigfússon (2009) showed that a significant amount of dissolved ions never leaves the column but forms secondary minerals almost instantly. Similar behavior can be expected to occur in nature. This

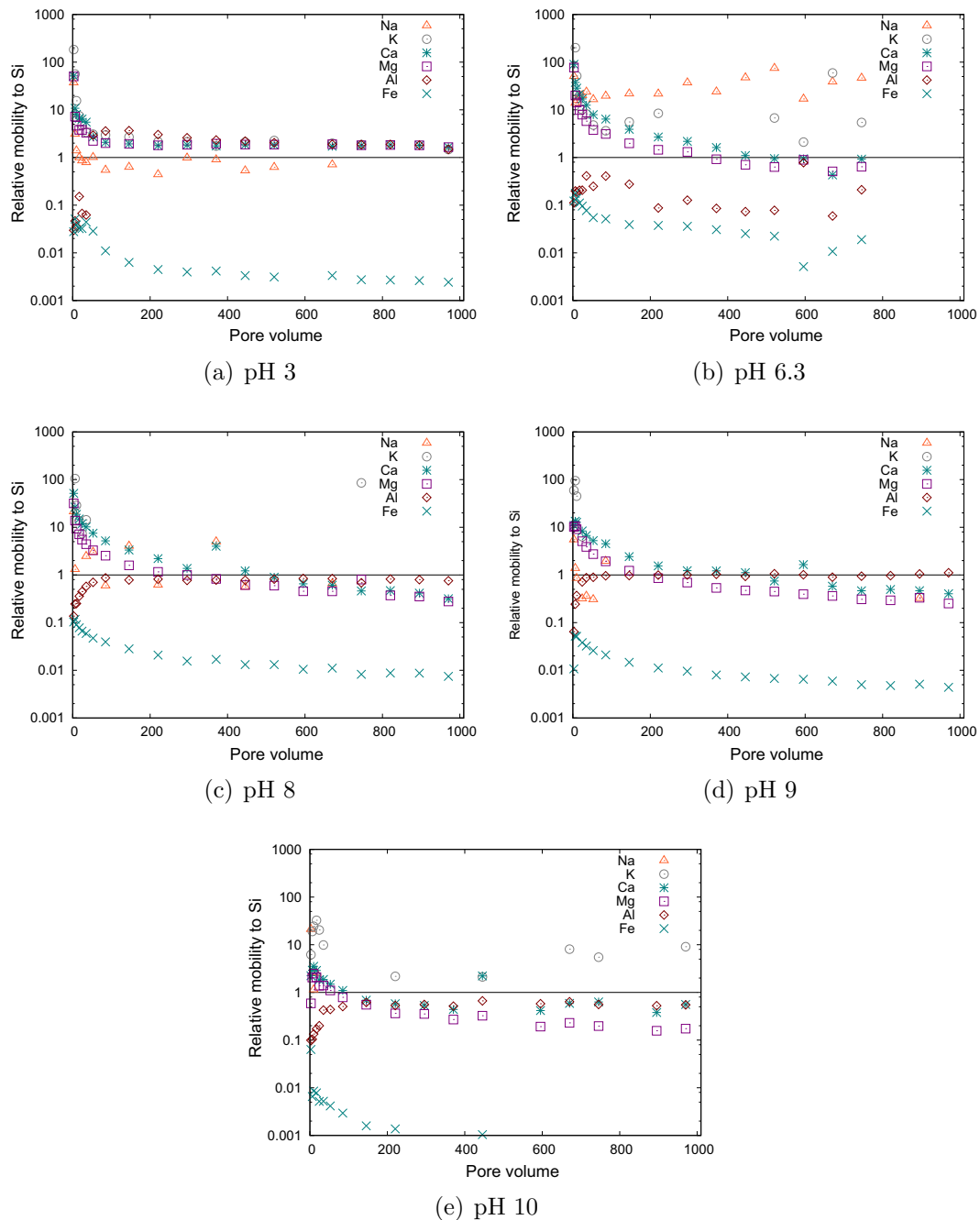


Fig. 10. Relative mobility of Na, K, Ca, Mg, Al and Fe with respect to Si in column outlet solutions.

raises the question on the practicality of the information gained from mixed flow reactor experiments carried out where minerals are strongly undersaturated, and using excessive water–rock ratio. Although results from such experiments may provide adequate information on dissolution mechanisms they are often extrapolated to conditions more relevant to water–rock interactions in nature without taking into account that precipitation of secondary minerals generally occurs rapidly under such conditions. Column flow through experiments provide a more realistic analog to natural water–rock interaction, e.g. with respect to water rock ratio and fluid transport, and should at least be carried

out in conjunction with mixed flow reactor experiments and consequently give results of more relevance to natural processes.

Figs. 6, 9 and 10 indicate low Fe mobility at most pH levels in column flow through experiments. At pH 3, Fe(III) vs. total Fe ratio is the same as for basaltic glass (10%) as shown in Fig. 9, which can be explained by negligible precipitation of secondary minerals at such a low pH. At pH 6.3, 8 and 9, however, only Fe(III) is released from the column while Fe(II) is retained within the column by incorporation into Fe-chlorite. As outlet Fe concentrations are close to zero at these pH levels, it is clear that Fe(III)

hydroxide did also precipitate within the column. However, some precipitated Fe(III) hydroxide particles are believed to have been small enough to have travelled as colloids through the filter at the end of the column, resulting in increased Fe(III) outlet concentrations. Recent studies have shown that Fe in colloids smaller than 0.22 μm in size can constitute between 1% and 60% of total Fe of particulate materials in river, lake and soil solutions (Ilna et al., 2013). These colloids would not affect the measured p_e by the Pt-electrode which always indicated lower p_e values than those calculated by the Fe(II)/Fe(III) redox couple (data not shown). At pH 10, Fe is still predominantly retained in Fe-chlorite and Fe(III) hydroxide within the column as can be seen in Fig. 6. However, Fe(III) is released in fractionally smaller amounts than at pH 6.3, 8 and 9 as can be seen in Fig. 9. Further studies are needed to explain this behavior, but redox disequilibrium is frequently observed in dilute solutions as those encountered in the present case (see e.g. Stefánsson et al., 2005).

The basaltic glass grains used in the column flow through experiments were found to have a large asperity on a 10–100 nm scale as shown in Fig. 4(b). This asperity clearly affects the reactivity of the glass but does not have the same effect on diffusion as diffusion through glass grains is effectively one-dimensional. As a result, it was decided to describe diffusivity within and through basaltic glass grains in the developed MINC model using geometric surface area that was calculated by assuming smooth spheres of diameter 187.5 μm , as described in Section 5.1. The chemical reactivity of the dissolving part of glass grains was however described using the BET surface area measured by Sigfússon (2009).

In the current study, basaltic glass was assumed to dissolve according to the rate law (1) published by Gíslason and Oelkers (2003). It is evident that the form of this rate law requires non-zero Al^{3+} activities, and given the potential for exceedingly low activities under neutral to basic pH values, a more general and computationally robust rate law was described by Maher et al. (2006) for Al-inhibition on plagioclase dissolution. The latter authors derive a hyperbolic form where the denominator tends to a formation constant as the dissolved Al species ($\text{Al}(\text{OH})_3$ in their discussion) goes to zero. Whereas, the rate law used in this manuscript is specific to the conditions of the basaltic glass dissolution experiments, and may not work well in other systems. Any form of rate law can be used in the MINC model approach described in this article.

Secondary mineral precipitation was assumed to take place only within the pore volume continuum of the MINC model. It is likely that some secondary mineral precipitation takes place in the gel layer, however given the limited thickness of the gel layer and its relatively low porosity, most of the dissolved species must pass through the layer before precipitating. Precipitation in the pore space also reduces the fluxes to the grain surface, because of the effect on diffusion through the bulk fluid. For example, if the MINC model is applied to a fracture through basaltic glass, the open space in the fracture would fill with secondary minerals, further limiting both advective and diffusive fluxes into the fracture and to the gel layer from the bulk solution. As

the fracture fills with secondary minerals, and the permeability decreases, the fluid in the fracture exchanges components with the bulk fluid primarily by diffusion, thus leading to a different local chemical environment.

The good agreement between simulated and measured column outlet concentrations in Fig. 6 shows that the MINC model can be used to simulate accurately relatively short-term experimental systems. However, further development of the MINC model is likely to be needed for it to be applicable to simulate processes occurring over geological time scales. Such development would have to involve moving boundaries, allowing for propagation of boundaries due to, e.g. grain shrinkage or growth, and possibly also re-definition of continua with time to account for, e.g. developing gradients within specific continua. One would also need to know which parameters control the long term dissolution rates of such basaltic glasses and how their dissolution would depend on intrinsic glass properties and environmental factors (see, e.g. Verney-Caron et al., 2011; Chave et al., 2011).

It is interesting to compare the MINC model presented in the current study to models developed for nuclear glasses, as it is generally accepted that basaltic and nuclear glasses behave similarly. Grambow and Müller (2001) developed a model describing nuclear waste glass corrosion both for experimental conditions as well as for a dynamic repository environment. The GRAAL model (glass reactivity with allowance for the alteration layer) was developed by Frugier et al. (2008) with the objectives of defining a rate law for glass alteration and describing the assemblage of amorphous and crystallized phases arising from glass alteration. Both models take microscopic effects into account by coupling explicitly the diffusion of mobile elements through a gel/leached layer and the thermodynamic equilibrium between the resulting hydrated and alkali depleted layer and the surrounding solution. The models have been implemented in geochemical simulators such as PhreeqC and Hytec and have been used for simulating the long-term behavior of nuclear glasses in contact with groundwater during the thousands of years necessary for decay of radionuclides in the glass structure. The Grambow and Müller model is similar to the MINC model to the extent that it describes penetration of water into the nuclear glass network by an advection/dispersion/reaction equation, typically used for mass transfer calculation of reactive transport in porous media. The GRAAL model, on the other hand, does not take advection into account. The MINC model would have to be modified in order to be capable of such long-term simulations. On the other hand, neither the Grambow and Müller model nor the GRAAL model allow for meshing the reaction zone from microscopic scale to macro (continuum) scale, which is one of the major strengths of the MINC model.

9. AD HOC ASSUMPTIONS AND UNCERTAINTIES ASSOCIATED WITH REACTIVE TRANSPORT MODELING

Large uncertainties are generally associated with reactive transport modeling, in part due to uncertainties in

laboratory measured values, but also due to lack of data and/or mathematical formulation of ongoing processes. Often one must thus accept significant uncertainties in parameters describing permeability, porosity, diffusivity, reactive surface area and mineral dissolution/precipitation rates. Hence, it follows that the results of reactive transport calculations can have uncertainties as high as several orders of magnitude. Much of this uncertainty can, however, be overcome by obtaining extensive and system specific physical and chemical parameters, as was done whenever possible in the current study. Nevertheless, several ad hoc assumptions had to be made with respect to thickness of different layers within basaltic glass grains (see discussion in Section 5.1). Other assumptions made are, e.g. related to secondary mineralogy as well as the surface areas and nucleation properties of precipitating minerals.

The selection of secondary minerals used in this study is based on an extensive review of natural analogs of water–basalt interaction as described in Section 5.2.1. Minerals that have commonly been reported to form during basalt alteration were thus compiled to the MINC model as no experimental data was available on exactly which secondary minerals in the flow through experiments simulated in the current study. A better understanding of reaction mechanisms, and in particular precipitation mechanisms, is an important factor in decreasing uncertainties associated with reactive transport modeling. Until more detailed formulations and data compatible with widely used numerical simulators will become available, geochemical model builders are forced to make critical assumptions such as the one that parameters for neutral pH dissolution rates also describe precipitation. More detailed data on surface areas of secondary minerals is also desperately needed but until it is available, one needs to assume their values. Sensitivity analysis carried out indicate changes in surface areas and hence reaction rates only to result in small changes in precipitated amounts as precipitation requires reactants whose availability is controlled by the slow dissolution of aluminosilicate minerals (see, e.g. Xu et al., 2005a).

10. SUMMARY AND CONCLUSIONS

The method of ‘multiple interacting continua’ (MINC) was applied to include microscopic processes in continuum scale reactive transport models of basaltic glass dissolution. The MINC method involves dividing the system up to ambient fluid and grains, using a specific surface area to describe the interface between the two. Four continua were used for describing a dissolving basaltic glass grain; the first one describes the ambient fluid around the grain, while the second, third and fourth continuum refer to the diffusive layer, the dissolving part of the grain and the inert part of the grain, respectively.

The model was validated using data from column flow through experiments of basaltic glass dissolution at low, neutral and high pH values. Good agreement between simulated and measured column outlet concentrations shows that the MINC model can be used for simulating accurately relatively short-term experimental systems. However,

further development of the MINC model is likely to be needed for it to be applicable to simulate processes occurring over geological time scales.

This study shows that reactive transport modeling can give further insight into experiments performed in laboratories or in the field, especially when dealing with dynamic processes and systems. Simulations of the column flow through experiment carried out by Sigfússon (2009) showed that a significant amount of dissolved ions never leaves the column but forms secondary minerals almost instantly. Non-stoichiometric experimental column outlet concentrations could thus be explained by precipitation of clay minerals, zeolites and hydroxides. Indications are, however, that simulated precipitation of stellerite was underestimated while precipitation of chlorite was overestimated. New information on precipitation kinetics and potential nonideality effects on thermodynamic equilibrium constants is likely to improve simulated results.

ACKNOWLEDGMENTS

We are grateful to Einar Gunnlaugsson, Gretar Ívarsson, Gunnar Gunnarsson and Ingvi Gunnarsson at Reykjavík Energy and Nic Spycher at Lawrence Berkeley National Laboratory for helpful discussions and support throughout this work. We also thank Andri Stefánsson, Helgi A. Alfredsson, Sigurdur R. Gíslason and Snorri Gudbrandsson at the Institute of Earth Sciences at the University of Iceland, Eric H. Oelkers at CNRS/Université Paul Sabatier in Toulouse and Andrew A. Meharg at the University of Aberdeen. We furthermore thank reviewers for their constructive comments and suggestions which greatly improved this paper.

This work was funded by the 7th Framework Programme of the EC (Project No. 283148), Reykjavík Energy, Geothermal Research Group GEORG (09-01-003 and 09-02-001) and the University fund of Eimskipafélag Íslands.

REFERENCES

- Accornero M. and Marini L. (2008) The double solid reactant method for modeling the release of trace elements from dissolving solid phases: I. Outline and limitations. *Environ. Geol.* **55**, 1627–2635.
- Advocat T., Chouchan J. L., Crovisier J. L., Guy G., Daux V., Jégou C., Gin S., Vernaz E. (1998) Borosilicate nuclear waste glass alteration kinetics: Chemical inhibition and affinity control. In *Mater. Res. Soc.* vol. 506, pp. 63–70.
- Aradóttir E. S. P., Sonnenthal E. L. and Jónsson H. (2012a) Development and evaluation of a thermodynamic dataset for phases of interest in CO₂ sequestration in basaltic rocks. *Chem. Geol.* **305–306**, 26–38. <http://dx.doi.org/10.1016/j.chemgeo.2012.01.031>.
- Aradóttir E., Sonnenthal E., Björnsson G. and Jónsson H. (2012b) Multidimensional reactive transport modeling of CO₂ mineral sequestration in basalts at the Hellisheiði geothermal field, Iceland. *Int. J. Greenhouse Gas Control* **9**, 24–40.
- Berger B., Claparols C., Guy C. and Daux V. (1994) Dissolution rate of a basalt glass in silica-rich solutions: Implications for long-term alteration. *Geochim. Cosmochim. Acta* **58**, 4875–4886.
- Bourcier W., Weed H., Nguyen S., Nielson J., Morgan L., Newton L. and Knauss K. (1992) Solution compositional effects on dissolution kinetics of borosilicate glass. *Mat. Res. Soc. Symp. Proc.* **176**, 209–216.

- Carroll S., Mroczek E., Alai M. and Ebert M. (1998) Amorphous silica precipitation (60 to 120 °C): Comparison of laboratory and field rates. *Geochim. Cosmochim. Acta* **62**, 1379–1396.
- Chave T., Frugier P., Gin S. and Ayrat A. (2011) Glass–water interphase reactivity with calcium rich solutions. *Geochim. Cosmochim. Acta* **75**, 4125–4139.
- Daux V., Guy C., Advocat T., Crovisier J. and Stille P. (1997) Kinetic aspects of basaltic glass dissolution at 90 °C: Role of aqueous silicon and aluminium. *Chem. Geol.* **142**, 109–126.
- Edwards A. L. (1972) *TRUMP: A Computer Program for Transient and Steady State Temperature Distributions in Multidimensional Systems*. National Technical Information Service, National Bureau of Standards, Springfield, VA.
- Frugier P., Gin S., Minet Y., Chave T., Bonin B., Godon N., Lartigue J., Jollivet P., Ayrat A., De Windt L. and Santarini G. (2008) SON68 nuclear glass dissolution kinetics: Current state of knowledge and basis of the new GRAAL model. *J. Nucl. Mater.* **380**, 8–21.
- Gíslason S., Heaney P., Oelkers E. and Schott J. (1997) Kinetic and thermodynamic properties of moganite, a novel silica polymorph. *Geochim. Cosmochim. Acta* **61**, 1193–1204.
- Gíslason S. and Oelkers E. (2003) Mechanisms, rates and consequences of basaltic glass dissolution: II. An experimental study of the dissolution rates of basaltic glass as a function of temperature. *Geochim. Cosmochim. Acta* **67**, 3817–3832.
- Grambow B. and Müller R. (2001) First-order dissolution rate law and the role of surface layers in glass performance assessment. *J. Nucl. Mater.* **298**, 112–124.
- Guy C. and Schott J. (1989) Multisite surface reaction versus transport during the hydrolysis of a complex oxide. *Chem. Geol.* **78**, 181–204.
- Iilina S., Poitrasson F., Lapitskiy S., Viers J. and Pokrovski O. (2013) Extreme iron isotope fractionation between colloids and particles of boreal and temperate organic-rich waters. *Geochim. Cosmochim. Acta* **101**, 96–111.
- Johnson J. W., Knauss K. G., Glassley W. E., DeLoach L. D. and Thompson A. F. B. (1998) Reactive transport modeling of plug-flow reactor experiments: Quartz and tuff dissolution at 240 °C. *J. Hydrol.* **209**, 81–111.
- Knauss K. G., Johnson J. W. and Steefel C. I. (2005) Evaluation of the impact of CO₂, co-contaminant gas, aqueous fluid and reservoir rock interactions on the geologic sequestration of CO₂. *Chem. Geol.* **217**, 339–350.
- Langmuir D. (1997) *Aqueous Environmental Geochemistry*. Prentice Hall, New Jersey.
- Lasaga A., Soler J., Ganor J., Burch T. and Nagy L. (1994) Chemical weathering rate laws and global geochemical cycles. *Geochim. Cosmochim. Acta* **58**, 2361–2386.
- Leturcq G., Berger G., Advocat T. and Vernaz E. (1999) Initial and long-term dissolution rates of aluminosilicate glasses enriched in Ti, Zr and Nd. *Chem. Geol.* **160**, 39–62.
- Lichtner P. C. (1996) Continuum formulation of multicomponent-multiphase reactive transport. *Rev. Mineral. Geochem.* **34**, 1–81.
- Maher K., Steefel C., DePaolo D. J. and Viani B. (2006) The mineral dissolution rate conundrum: Insights from reactive transport modeling of U isotopes and pore fluid chemistry in marine sediments. *Geochim. Cosmochim. Acta* **70**, 337–363.
- Marini L. (2007) *Geological Sequestration of Carbon Dioxide – Thermodynamics, Kinetics and Reaction Path Modeling*. Elsevier, Amsterdam.
- Narasimhan T. and Witherspoon P. (1976) An integrated finite difference method for analyzing fluid flow in porous media. *Water Resour. Res.* **12**, 57–64.
- Nesbitt H. W. and Skinner W. M. (2001) Early development of Al, Ca, and Na compositional gradients in labradorite leached in pH 2 HCl solutions. *Geochim. Cosmochim. Acta* **65**, 715–727.
- Oelkers E. and Gíslason S. (2001) The mechanism, rates and consequences of basaltic glass dissolution: I. An experimental study of the dissolution rates of basaltic glass as a function of aqueous Al, Si and oxalic acid concentrations at 25 °C and pH = 3 and 11. *Geochim. Cosmochim. Acta* **65**, 3671–3681.
- Palandri J., Kharaka Y. (2004) A compilation of rate parameters of water–mineral interaction kinetics for application to geochemical modeling. Report 2004-1068.
- Paul A. (1977) Chemical durability of glasses, a thermodynamic approach. *J. Mater. Sci.* **12**, 2246–2268.
- Pruess K. and Narasimhan T. N. (1985) A practical method for modeling fluid and heat flow in fractured porous media. *Soc. Petrol. Eng. J.* **25**, 14–26.
- Rimstidt J. D. and Barnes H. L. (1980) The kinetics of silica–water reactions. *Geochim. Cosmochim. Acta* **44**, 1683–1699.
- Sigfússon B. (2009) Reactive transport of arsenic through basaltic porous media. Ph. D. thesis, Univ. Aberdeen.
- Sigfússon B., Meharg A. and Gíslason S. (2008) Regulation of arsenic mobility on basaltic glass surfaces by speciation and pH. *Environ. Sci. Technol.* **42**, 8816–8821.
- Steefel C. and Lasaga A. (1994) A coupled model for transport of multiple chemical species and kinetic precipitation/dissolution reactions with applications of reactive flow in single phase hydrothermal systems. *Am. J. Sci.* **294**, 529–592.
- Stefánsson A. and Gíslason S. (2001) Chemical weathering of basalts, Southwest Iceland: Effect of rock crystallinity and secondary minerals on chemical fluxes to the ocean. *Am. J. Sci.* **301**, 513–556.
- Stefánsson A., Arnórsson S. and Sveinbjörnsdóttir A. (2005) Redox reactions and potentials in natural waters at disequilibrium. *Chem. Geol.* **221**, 289–311.
- Techer I., Advocat T., Lancelot J. and Liotard J. (2001) Dissolution kinetics of basaltic glasses: Control by solution chemistry and protective effect of the alteration film. *Chem. Geol.* **176**, 235–263.
- Verney-Caron A., Vigier N. and Millot R. (2011) Experimental determination of the role of diffusion on Li isotope fractionation during basaltic glass weathering. *Geochim. Cosmochim. Acta* **75**, 3452–3468.
- Wolery T. (1992) EQ3/6: Software package for geochemical modeling of aqueous systems: Package overview and installation guide (version 7.0). Report UCRL-MA-210662. Lawrence Livermore National Laboratory, Livermore, Calif.
- Wolff-Boenisch D., Gíslason S. and Oelkers E. (2004) The effect of fluoride on the dissolution rates of natural basaltic glasses at pH 4 and 25 °C. *Geochim. Cosmochim. Acta* **68**, 4571–4582.
- Xu T. and Pruess K. (2001) Modeling multiphase non-isothermal fluid flow and reactive geochemical transport in variably saturated fractured rocks: 1. Methodology. *Am. J. Sci.* **301**, 16–33.
- Xu T., Sonnenthal E., Spycher N., Pruess K., Brimhall G. and Apps J. (2001) Modeling multiphase non-isothermal fluid flow and reactive geochemical transport in variably saturated fractured rocks: 2. Applications to supergene copper enrichment and hydrothermal flows. *Am. J. Sci.* **301**, 34–59.
- Xu T., Apps J. A. and Pruess K. (2005a) Mineral sequestration of carbon dioxide in a sandstone-shale system. *Chem. Geol.* **217**, 295–318.
- Xu T., Sonnenthal E., Spycher N., Pruess K. (2005b) TOUGH-REACT User's Guide: A simulation program for non-isothermal multiphase reactive geochemical transport in variably saturated geologic media. LBNL-55460. Lawrence Berkeley National Laboratory, Berkeley, Calif.
- Xu T., Sonnenthal E., Spycher N. and Pruess K. (2006) TOUGH-REACT – A simulation program for non-isothermal multiphase reactive geochemical transport in variably saturated

- geologic media: Applications to geothermal injectivity and CO₂ geologic sequestration. *Comput. Geosci.* **32**, 146–165.
- Xu T., Kharaka Y. K., Doughty C., Freifeld B. M. and Daley T. M. (2010) Reactive transport modeling to study changes in water chemistry induced by CO₂ injection at the Frio-I Brine Pilot. *Chem. Geol.* **271**, 153–164.
- Xu T., Spycher N., Sonnenthal E., Zhang G., Zheng L. and Pruess K. (2011) TOUGHREACT version 2.0: A simulator for subsurface reactive transport under non-isothermal multiphase flow conditions. *Comput. Geosci.* **37**, 763–774.
- Zimmerman R. W., Chen G., Bodvarsson G. S. (1992) A dual-porosity reservoir model with an improved coupling term. In: *Proceedings, Seventeenth Workshop on Geothermal Reservoir Engineering*, Stanford University, Stanford, California, January 29–31, 1992.

Associate editor: C. Steefel